Author version: *ICES J. Mar. Sci., vol.68(4); 2011; 745-750*

Aerosol optical thickness and spatial variability along coastal and offshore waters of the eastern Arabian Sea

Harilal B. Menon, Nutan Sangekar, Aneesh Lotliker, Krishnaswamy Krishnamoorthy, and Ponnumani Vethamony

Data from the ocean-colour monitor (OCM), on board the Indian Remote Sensing Satellite (IRS) P4, were used to analyse the spatial and temporal distribution of aerosol optical thickness (AOT) over the coastal and offshore waters of the eastern Arabian Sea. Zero water-leaving radiance from the near infrared (NIR) region was assumed for oceanic (open ocean) waters, because of the absorption of long-wave radiation by water molecules. Because this assumption fails in coastal waters, we corrected for water-leaving radiance and sun glint to the NIR bands. The aerosol size-distribution parameter (α) was derived from a relationship between two NIR bands. The Angström turbidity parameter (β) was obtained using an algorithm relating *in situ* hand-held, sun-photometer measurements and aerosol radiance (L_a) at 490 nm. The relationship between β and L_a (490) was obtained with a sensitivity analysis, using a calibrated radiative transfer model. AOTs were retrieved for each pixel of 500 nm. The performance of the algorithm was tested by comparing OCM-derived AOT values with *in situ* AOT and MODIS-derived values. Aerosol maps thus generated from January to December 2005 demonstrate the potential of this new retrieval method for producing aerosol optical-thickness climatology from OCM data over coastal waters.

Keywords: Aerosol optical thickness, coastal waters, eastern Arabian Sea, offshore, spatial variability

Running title: Arabian Sea aerosol optical thickness and variability

Received 28 June 2010; accepted 22 October 2010.

H. B. Menon, N. Sangekar, and A. Lotliker: Department of Marine Sciences, Goa University, University PO, Goa, 430 206, Indi; K. Krishnamoorthy: Space Physics Laboratory, Vikram Sarabhai Space Centre, Thiruvananthapuram, Kerala, India; P. Vethamony: National Institute of Oceanography, Dona-Paula, Goa, 403004, India.

Correspondence to: H. B. Menon: tel: +91 832 651 9350; fax: +91 832 245 1184; e-mail: harilalm@gmail.com

Introduction

The atmosphere above the North Indian Ocean is subject to aerosol radiative forcing resulting from seasonally reversing summer (southwest) and winter (northeast) monsoon winds. Several Indian programmes have been initiated to understand the direct and indirect effect of these aerosols on climate. Analysis of data from the Indian Ocean Experiment (INDOEX: 1997–1999; Ramanathan *et al*., 2001) revealed northeast monsoon winds as the main agent transporting anthropogenic aerosols over the Arabian Sea. These aerosols, unlike natural maritime aerosols, not only scatter incoming solar radiation, but also absorb it (Satheesh and Ramanathan*,* 2000*;* Eck *et al*., 2001; Li and Ramanathan, 2002) and augment the greenhouse effect. This disclosure motivated an extensive field campaign (Integrated Campaign for Aerosols, Gases, and Radiation Budget (ICARB) in 2006 (Krishnamoorthy *et al.*, 2008**).** The combined effect of natural and anthropogenic aerosols could contribute to atmospheric and ecological imbalances in the eastern Arabian Sea. This underlines the necessity of a synoptic understanding of the atmosphere over the eastern Arabian Sea, including the Angström turbidity parameter (β), aerosol-size distribution parameter (α), and subsequently aerosol optical thickness (AOT), an important quantity required for determining aerosol radiative forcing at the top of the atmosphere.

The role of aerosols in climate change remains uncertain. Although the theory behind their effect on outgoing terrestrial and incoming solar radiations is well understood, spatial and temporal variability make it difficult to assess their magnitude with *in situ* observations. Satellite remote sensing is the only means of providing the synoptic coverage needed for analysing aerosol radiative forcing at the top of the atmosphere. Rajeev and Ramanathan (2002) discussed spatial distribution of AOT over the open ocean (Arabian Sea and Bay of Bengal) at a spatial resolution of 1.1 km, using data for the 630 nm band of Advanced Very High Resolution Radiometer (AVHRR) onboard National Oceanic and Atmospheric Administrations (NOAA) satellite. However, an analysis of the small-scale features associated with aerosol distribution over optically complex areas, such as the coastal waters of the eastern Arabian Sea, requires sensors with higher temporal and spatial resolutions. The ocean-colour monitor (OCM), on board the Indian Remote Sensing Satellite P4, provides spatial and temporal resolutions of 360 m and 2 d, respectively. Previous attempts to retrieve AOT from OCM data over the eastern Arabian Sea (Indrani Das *et al.,* 2002; Dey *et al.,* 2004; Chauhan *et al.,* 2009) assumed that sensor radiance of NIR bands resulted entirely from atmospheric backscattering. However, this assumption holds only in oceanic and not in turbid coastal waters. The current study aims to formulate a technique to derive AOT from OCM

over coastal waters and to demonstrate the method's potential for analysing aerosol distribution along the eastern coastal Arabian Sea. In the fisheries context, these AOT values could be used to estimate aerosol radiance as a part of the complex atmospheric correction procedure, resulting in more accurate chlorophyll *a* values.

Material and methods

Study area and data collection

The AOT over oceanic and coastal regions of the eastern Arabian Sea (Figure 1), including the estuaries of Mandovi and Zuari (Goa, India), was studied as part of the Indian Space Research Organization's Geosphere Biosphere Programme. Oceanic observations were obtained from the RV "Sagar Kanya" in an area bounded by 14°20'–22°35'N and 65°–73°34'E during 4–18 December 2004. Coastal waters were surveyed by the RV "Sagar Purvi" during 23–28 November 2004. Six estuarine surveys were conducted using a fishing vessel on 12 February, 18 March, 13 April, 11 May, 11 November, and 9 December 2005.

A Microtops II hand-held sun photometer, with bands at 380, 440, 500, 675, and 870 nm, was used to measure AOT (full field view of 2.5°). A global positioning system (GPS) interfaced with the Microtops II provided accurate time and position of each station. During all the field surveys, AOTs were measured between 09:00 and 16:00 at 30-min intervals, in association with the IRS P4 satellite pass (12:00). This provided a total of 210, 78, and 90 observations for the oceanic, coastal, and estuarine surveys, respectively.

Predetermined stations (Figure 1) for *in situ* observations were located between depths of 30 and 1000 m (8–700 km from shore) to prevent water-pixel contamination from land radiance. Profiles of downwelling irradiance and upwelling radiances were obtained with a Satlantic in-water radiometer at all stations. In addition, surface water samples were collected to determine the concentration of optically active substances (OAS), including suspended organic (chlorophyll *a*), inorganic (sediment), and chromophoric dissolved organic (CDOM) matter, using methods described by Menon *et al*. (2005). Radiometer measurements and water sample collection were carried out simultaneously from the sunlit side of the ship to avoid any discrepancy in the computation of water-leaving radiance resulting from of a change in sun-zenith angle.

Generation of α and β from *in situ* measurements

According to Angström (1961), the spectral variation of AOT is expressed as

$$\tau_a(\lambda) = \beta \lambda^{-\alpha}, \quad (1)$$

where $\tau_a(\lambda)$ is the aerosol optical thickness, β [often referred to as the Angström turbidity parameter (Angström, 1964)] represents the aerosol optical thickness at the reference wavelength (i.e. $\lambda = 1$), which may be viewed as an indicator of total aerosols present in the atmosphere, and α is the Angström coefficient, which depends on the size distribution of the aerosol**.** Each spectral measurement of aerosol optical thickness was fitted to Equation (1) using linear least-squares fitting of log-transformed data, to obtain α as the slope of the regression line and log β as the intercept. Low and high values of α indicate coarse (maritime) and fine (continental) aerosol particle sizes, respectively.

OCM characteristics and data processing

OCM data from the IRS P4 satellite were analysed to retrieve AOT. OCM has eight bands; six visible and two near infrared (NIR), centred at 412, 443, 490, 510, 555, 670, 765, and 865 nm. The first six bands are used for analysing the OAS (ocean-colour components) in the water column and the remaining two bands for measuring path radiance (aerosol and Rayleigh radiances), to apply atmospheric correction for ocean-colour analysis. The spectral resolution of the visible and NIR bands are 20 and 40 nm, respectively.

Images were georeferenced using ground control points and the study area was extracted using image processing software. During November–January, because the aerosol plume builds around 22°N, two OCM images were processed to include the area between 10 and 23°N. For the remaining months, only one image, covering the area between 5 and 20°N, was processed. Cloud cover prevented analysis of aerosol parameters during June–August**.** To validate the AOT retrieval method from OCM further, AOTs derived seasonally from OCM pixels over oceanic waters (8–15°N) were compared with AOTs from MODIS. This comparison was made between mean of nine adjacent pixels of AOT from OCM and the corresponding pixels of MODIS.

Aerosol retrieval from OCM data

The radiance received by a space-borne optical sensor from a turbid coastal waterbody in a specific band λ can be divided into different components as

$$L_t(\lambda) = L_p(\lambda) + t\,(\lambda) \times L_g(\lambda) + L_w(\lambda) \times T_d(\lambda), \qquad (2)$$

where $L_p(\lambda)$ is the path radiance resulting from aerosol and Rayleigh scattering in the atmosphere, $L_g(\lambda)$ is the sun glint resulting from specular reflection from the sea surface, and $L_w(\lambda)$ is the radiance leaving the water column. $T_d(\lambda)$ and $t(\lambda)$ are the diffuse and direct transmittance terms.

Aerosol radiance, a component of path radiance, contains information on the atmospheric aerosol. To retrieve β from aerosol radiance, the atmospheric path radiance L_p of NIR bands must be partitioned into aerosol (L_a) and Rayleigh (L_r), radiances as follows:

$$L_p\,(\lambda) = L_a\,(\lambda) + L_r\,(\lambda). \qquad (3)$$

Rayleigh radiance [$L_r\,(\lambda)$] was computed as per Gordon (1988) and removed from L_p of NIR bands**.** Because water molecules absorb long-wave radiation, Rayleigh correction to pixels of NIR bands should yield L_a over oceanic waters. However, $L_w\,(\lambda)$ in NIR bands from the turbid coastal waters is non-zero (Moore *et al*., 1999). In addition, radiance resulting from specular reflection [sun glint, $L_g\,(\lambda)$] contributes to radiance measured in the NIR bands. Therefore, $L_r\,(\lambda)$, $L_w\,(\lambda)$, and $L_g\,(\lambda)$ correction should be applied to NIR bands. $L_g\,(\lambda)$ correction was applied to the NIR bands as per Wang and Bailey (2001). Wind velocity for the computation of sun glint was measured using an automatic weather station (AWS) installed on board the ship.

The water-leaving radiance correction to 765 nm pixels was applied using the remote-sensing reflectance (R_{rs}) at 765 nm [$R_{rs}(765)$], measured from the *in situ* radiometer measurements. The OAS effect on R_{rs} at 865 nm was computed using a calibrated radiative-transfer model (Menon, 2004) because the Satlantic radiometer does not have a band at this wavelength. Although the data revealed a direct relationship between reflectance and OAS concentration at 765 nm, this was not the case for the 865 nm band. Suspended organic and inorganic particles scatter and absorb light, whereas dissolved components only absorb it (Bricaud *et al.*, 1981; Menon *et al.,* 2005). A multiple regression analysis of R_{rs} (765) with OAS components revealed that neither chlorophyll *a* nor CDOM affects R_{rs} (765), but that suspended

sediment contributes to it at concentrations >4 mg l^{-1}. The water-leaving radiance at 4 mg l^{-1} is 0.0184 μW m^{-2} nm sr^{-1}. At 765 nm, this gives

$$L_u(0^+, 765) = R_{rs}(0^+, 765) \times E_d(0^+, 765), \quad (4)$$

where $L_u(0^+, 765)$ is the upwelling radiance at the water surface, $R_{rs}(0^+, 765)$ is the remote-sensing reflectance, and $E_d(0^+, 765)$ is the downwelling irradiance at 765 nm at the water surface. $E_d(0^+, 765)$ and $L_u(0^+, 765)$ were obtained from the Satlantic radiometer.

Pixels with sediment concentration >4 mg l^{-1} were corrected as follows. For pixels coinciding with station positions, the water-leaving radiance correction was applied by computing the respective radiance; for other pixels, the correction was applied to the mean of nine pixels adjacent to the station. Aerosol radiance (L_a) thus obtained could be expressed as

$$L_a(\lambda) = F_s(\lambda)\, \tau_a(\lambda)\, \omega_{oa} \times P_a/4\pi \cos(\theta_v), \quad (5)$$

where $F_s(\lambda)$ is the extraterrestrial solar irradiance, $\tau_a(\lambda) = \beta\, \lambda^{-\alpha}$ is the AOT, ω_{oa} is the aerosol single-scattering albedo, P_a is the aerosol phase function, and θ_v is the satellite view angle. Assuming that phase function and single-scattering albedo are spectrally invariant at a specific time over the short range of wavelength considered (765–865 nm), and taking the ratio of Equation (6) for the two NIR bands of OCM, results in the following relation that can be used to map α from OCM

$$\alpha = [\log(L_{a1}/F_{s1}) - \log(L_{a2}/F_{s2})]/[\log(\lambda_2) - \log(\lambda_1)], \quad (6)$$

where L_{a1} and L_{a2} are aerosol radiances corresponding to 765 and 865 nm, respectively, and F_{s1} and F_{s2} are the respective extraterrestrial solar irradiances. Another parameter required for the retrieval of AOT is β, the Angström turbidity parameter.

An algorithm was developed using results from a sensitivity analysis of a radiative-transfer model (Menon, 2004) to retrieve β from OCM, as follows. Spectral (400–700 nm) aerosol radiances (L_a) were computed at 1-nm intervals for the range of β values (0.1–0.4) encountered over an Indian coastal station. While simulating aerosol radiances, the following variables α, zenith angle, azimuth angle, atmospheric gaseous constituents, and OAS were held constant. Approximately 200 spectra of aerosol radiances were simulated for the wavelength range. The L_a, corresponding to the least β, was taken as

the baseline spectrum; all other L_a spectra were then divided by this baseline. This demonstrated that maximum sensitivity to change in β occurs at 490 nm. The following linear relationship was then obtained between satellite L_a (490) and *in situ* derived β ($r^2 = 0.95$, Figure 2):

$$\beta = 0.1925\, L_a(490) - 0.0242. \qquad (7)$$

In situ data for alternate days were grouped into two sets and used for developing the algorithm and validating it. Altogether, 125 observations were used. Of these, 75 were generated during the RV "Sagar Kanya" survey and 25 each from the RV "Sagar Purvi" and fishing vessel surveys. Next, L_a (490) from OCM was obtained by rearranging the ratio of Equation (7) for 765 nm and shorter wavelengths, therefore allowing computation of L_a for these wavelengths

$$L_a (\lambda < 765 \text{ nm}) = L_a (765 \text{ nm}) [F_s (\lambda)/F_s (765 \text{ nm})] [(\lambda/765)^{-\alpha}], \qquad (8)$$

where α is the value obtained using Equation (7) derived from satellite data.

Nine OCM images (10 January, 12 February, 18 March, 11 April, 11 May, 20 September, 6 October, 25 November, and 12 December 2005) were then processed to retrieve α and β parameters. The Angström equation (1961) was then applied and AOTs and α at 500 nm were mapped.

Validation

A total of 150 observations (90, 45, and 15 from the RV "Sagar Kanya", RV "Sagar Purvi", and fishing vessel surveys, respectively) was used for validation of satellite-derived values**.** Each pixel contained more than one *in situ* value. Hence, average of α and β were compared with mean values of the adjacent nine pixels in the satellite imagery. To avoid possible land interference (estuarine width decreases upstream), only those observation taken at the mouth were considered for validation.

To authenticate the method further, AOTs derived seasonally from OCM cloud-free pixels in an open-ocean region between 8 and 15°N (not in the area of *in situ* observations) were compared with AOTs from MODIS. MODIS has a 550 nm band; consequently, AOTs from OCM-derived α and β at 550 nm were used for the comparison.

Results and discussion

Validation

In general, OCM-derived products and *in situ* observations are in good agreement and in the same range (Figure 3a–c). In particular, there was good agreement between satellite-derived and *in situ* AOT values (Figure 3c). The confidence level, RMS error, and mean difference bias were computed for this relationship and were 95, 2.267, and 0.965%, respectively. Moreover, the zero offset and slope close to unity supports the accuracy of the retrieval. There was also good agreement between OCM- and MODIS-derived AOTs during the pre-monsoon (February–May), end of monsoon (September) and post-monsoon (October–January) seasons (Figure 4a–c).

Aerosol distribution

The spatial distribution of satellite-derived AOT during January–December (Figure 5a) reveals an inter- and intraseasonal variability over the study area. AOT is significantly higher during the pre- (January–May) than in the post-monsoon (September–December) season. Aerosol plumes originating in the western margin of the Indian subcontinent extend deep into the offshore region during the pre-monsoon, with AOT ranging from 0.2 to 0.5.

A low AOT (0.15) at the northeastern region and a high AOT (0.4) along the coast between 15 and 20°N are the significant features during January. AOT values increased farther offshore during this month and by February formed an offshore aerosol plume. Except for this localized plume, aerosol distribution was spatially uniform (~0.3) in February. During March, aerosol in the inshore region around 20°N 72°E increased and the offshore plume strengthened further. Three hotspots were then evident**,** one inshore and two offshore, all oriented northeast–southwest in narrow plumes. By April, these had merged into a single elongated plume with the same orientation. By May, this plume had dissipated into patches of intermittent low and high values along the coast and offshore. Examination of wind patterns from NCEP/NCAR reanalysis data (a joint product from the US National Centers for Environmental Prediction and the National Center for Atmospheric Research) revealed that the northerly winds during January had changed to northeasterly by April, suggesting that changes in wind direction caused these changes in aerosol distribution. During winter, strong northeast monsoon winds maintain a vertical moisture gradient by bringing dry, continental air over the eastern Arabian Sea, thereby allowing

continued intense evaporation (Prasannakumar *et al.,* 2001). This results in increased atmospheric humidity and subsequent atmospheric convection. Increased humidity increases aerosol particle size because of hygroscopic growth (Im *et al.,* 2001). This augments scattering, resulting in increased optical thickness. This process might cause the high AOT (0.5) values at the plume's core. In their studies, Li and Ramanathan (2002) noted that AOT is high over both the Arabian Sea and the Bay of Bengal during the northeast monsoon. They observed aerosol plumes over the Arabian Sea and attributed them to the advection of continental anthropogenic emissions. Similar results were obtained in a study examining the role of synoptic and mesoscale weather patterns on aerosol spectral optical depths and size characteristics at a coastal industrial site in India (Niranjan *et al.,* 2004).

The aerosol pattern during May could be explained based on changing wind direction. The Findlater Jet (also known as the Somali Jet) originates around 10°S and progresses northward as the southwest monsoon advances. It then becomes southwesterly to westerly while crossing the equator (Menon, 1989). It intensifies by May and begins to blow from the African continent in a southwesterly–westerly direction, resulting in the observed redistribution of aerosol along the coast. Studies in the southern Arabian Sea demonstrated that during May, southwesterly–westerly winds bring mineral dust from Arabia and North Africa (Li and Ramanathan, 2002)**.** The type of aerosol over the study area is indicated by the temporal distribution of the aerosol size distribution parameter (α; Figure 5b). Low values for α and the large optical thickness along the coast clearly indicate enhanced loading of mineral dust aerosols during May compared with earlier months. However, this could be supplemented by coarse mode marine aerosols generated and transported by westerly winds, which increase as the monsoon approaches.

Removal of aerosol because of widespread monsoonal rains from June to August depletes the AOT by September. Wind patterns are intermediate in October, during the initial phase of the transition from southwest to northeast monsoons. This causes an uneven distribution of aerosol along the coast during October (Figure 5a). By the end of November, northeast monsoon winds become more unidirectional, resulting in the concentration of aerosol off 22°N 68°E (Figure 5a). Although AOT decreases gradually towards the south, a patch of aerosol with AOT = 0.5 is seen around 7°N, which could be attributed to sea salt aerosol**.** In their studies, Li and Ramanathan (2002) indicated an enhancement in the production of sea salt because of wind. In December, the wind pattern becomes

uniform and the plume seen off 22°N and 68°E further strengthens and concentrates in a northeasterly–southwesterly direction.

Conclusions

In the fisheries context, satellite remote sensing of phytoplankton biomass and its temporal and spatial variability of Indian coastal waters is essential to the country's potential fishing zone (PFZ) programme and other initiatives in fishery oceanography using ocean-colour data. However, to obtain accurate chlorophyll *a* measurements as an index of phytoplankton biomass from an optical sensor, corrections for atmospheric effects must be implemented. The current study develops a new algorithm to retrieve aerosol parameters α and β from OCM to compute AOT over coastal turbid waters. These AOT values can be used to estimate aerosol radiance as a part of the complex atmospheric correction procedure resulting in more accurate chlorophyll *a* values.

Acknowledgements

The authors thank the Indian Space Research Organization for funding the project under the IGBP programme and Professor Dilip Debgaokar, Vice Chancellor, Goa University, for constant encouragement during this study.

References

Angström, A. 1964. The parameters of atmospheric turbidity. Tellus, 16: 64–75.

Bricaud, A., Morel, A., and Prieur, L. 1981. Absorption by dissolved organic matter of the sea (yellow substance) in the UV and visible domains. Limnology and Oceanography, 26: 43–53.

Chauhan, P., Sanwlani, N., and Navalgund R. R. 2009. Aerosol optical depth variability in the Northeastern Arabian Sea during winter monsoon: a study using in-situ and satellite measurements. Indian Journal of Marine Science, 38: 390–396.

Das, I., Mohan, M., and Krishnamoorthy, K. 2002. Detection of Marine aerosols with IRS–P4–OCM. Proceedings of Indian Academy of Sciences (Earth & Planetary Science), 111: 425–435.

Dey, S., Sarkar, S., and Singh, R. P. 2004. Comparison of aerosol radiative forcing over the Arabian Sea and Bay of Bengal. Advances in Space Research. 33, 1104–1108.

Eck, T. F., Holben, B. N., Dubivik, O., Smirnov, A., Slutsker, I., Lobert, J. M., and Ramanthan, V. 2001. Column-integrated aerosol optical properties over the Maldives during the northeast monsoon for 1998–2000. Journal of Geophysical Research, 106: 28 555–28 566.

Gordon, H. R., Brown, J. W., and Evans, R. H. 1988. Exact Rayleigh scattering calculations for use with the Nimbus-7 Coastal Zone Color Scanner. Applied Optics, 27: 862–871.

Im, J., Saxena, V. K., and Wenny, B. N. 2001. An assessment of hygroscopic growth factors or aerosols in the surface boundary layer for computing direct radiative forcing. Journal of Geophysical Research, 10: 20 213–20 224.

Krishnamoorthy, K., Satheesh, S. K., Suresh Babu, S., and Dutt, C. B. S. 2008. Integrated Campaign for Aerosols, gases and Radiation Budget (ICARB): An overview. Journal of Earth System Science, 117: 243–262.

Li, F., and Ramanathan, V. 2002. Winter to summer monsoon variation of aerosol optical depth over the tropical Indian Ocean. Journal of Geophysical Research, 107: doi: 10.1029/2001JD000949.

Menon, H. B. 2004. Calibration of an optical equation to analyse the atmosphere turbidity and water quality of an estuarine environment. Journal of Indian Society of Remote Sensing, 32: 287–300.

Menon, H. B., Lotliker, A. A., and Nayak, S. R. 2005. Pre-monsoon bio-optical properties in estuarine, coastal and Lakshadweep waters. Estuarine Coastal and Shelf Science, 63: 211–223.

Menon, P. A. 1989. Our Weather. National Book Trust, India. 121 pp.

Moore, G. F., Aiken, J., and Lavender S. J. 1999. The atmospheric correction of water colour and the quantitative retrieval of suspended particulate matter in case 2 waters applications to MERIS. MERIS special issue. International Journal of Remote Sensing, 20: 1713–1737.

Niranjan, K., Malleswara, B. R., Saha, A., and Murty, K. S. R. 2004. Aerosol spectral optical depths and size characteristics at a coastal industrial location in India–effect of synoptic and mesoscale weather. Annales Geophysicae, 22: 1851–1860.

Prasannakumar, S., Ramaiah., N., Gauns, M., Sarma V. V. S. S., Muralidharan, P. M., Raghukuar, S., Dilipkumar, M., and Madhupratap, M. 2001. Physical forcing of biological productivity in the Northern Arabian Sea during the North east monsoon season. Deep Sea Research Part II, 48: 1115–1126.

Rajeev, K., and Ramanathan, V. 2002. The Indian Ocean Experiment: Aerosol Forcing obtained from Satellite data. Advances in Space Research, 29: 1731–1740.

Ramanathan, V., Crutzen, P. J., and Lelieveld, J. 2001. Indian Ocean Experiment: An integrated analysis of the climate forcing and effects of the great Indo-Asian haze. Journal of Geophysical Research, 106: 28 371–28 398.

Satheesh, S. K., and Ramanathan, V. 2000. Large differences in tropical aerosol forcing at the top of the atmosphere and Earth's surface. Nature, 405: 60–63.

Wang, M., and Bailey, S. W. 2001. Correction of sun-glint contamination on the SeaWiFS ocean and Atmosphere products. Applied Optics, 40: 4790–4798.

Figure 1. Map of study area illustrating *in situ* sampling locations and depth contours. Main panel: oceanic observations, RV "Sagar Kanya"; top inset: estuarine observations, fishing trawler; bottom inset: coastal observations, RV "Sagar Purvi".

Figure 2. Regression between *in situ* β (Angstöm turbidity parameter) and satellite-derived L_a 490 (aerosol radiance at 490 nm).

Figure 3. Correlation between (a) satellite- and *in situ*-derived α (aerosol size distribution parameter); (b) satellite-derived and *in situ* β (Angström turbidity parameter); (c) satellite-derived AOT and *in situ* values for validation. Dotted lines in (a) and (b) – 95% confidence level; vertical and horizontal bars – s.d.

Figure 4. Correlation between AOT at 550 nm derived from OCM and MODIS for (a) pre-monsoon, (b) monsoon, and (c) post-monsoon seasons.

Figure 5. Spatial distribution of (a) AOT at 500 nm and (b) α derived with Ocean Colour Monitor (OCM) data for 10 January, 12 February, 18 March, 11 April, 11 May, 20 September, 6 October, 26 November, and 10 December 2005.

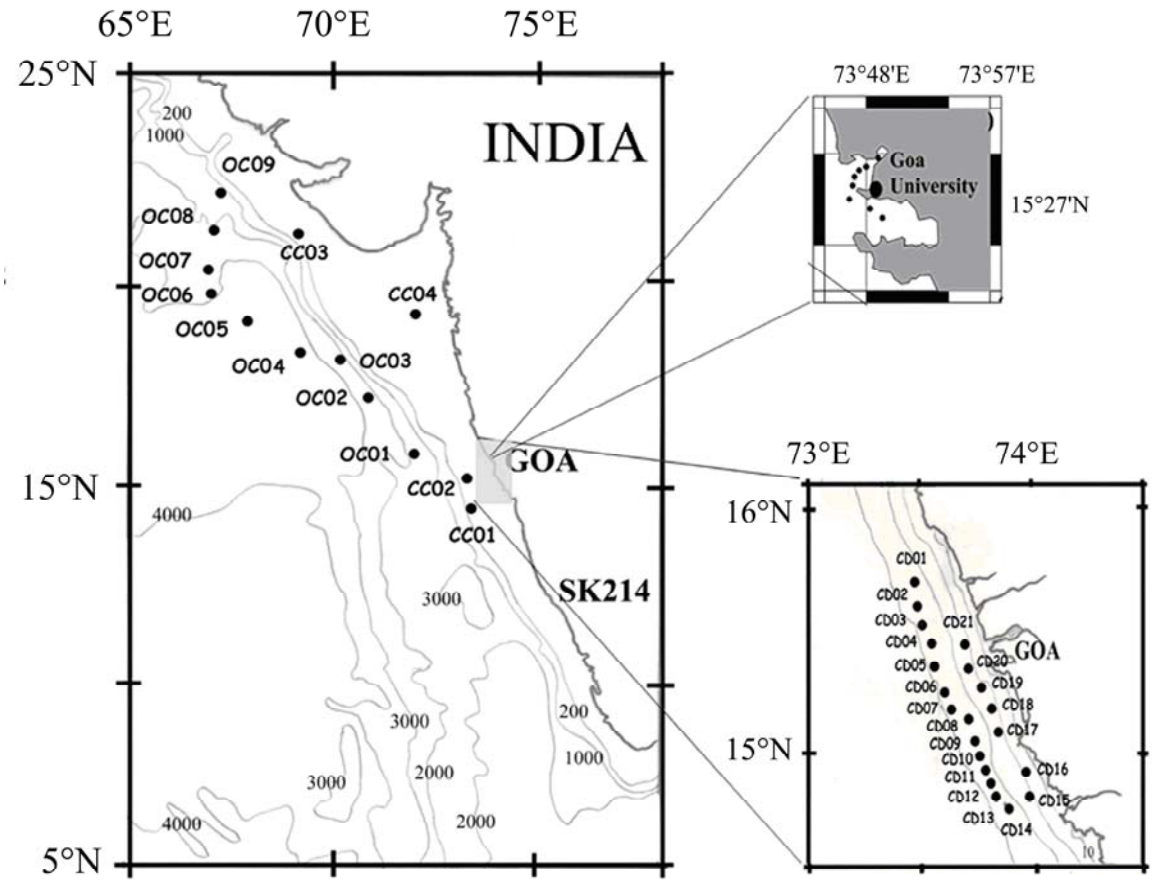

Figure 1. Map of study area illustrating *in situ* sampling locations and depth contours. Main panel: oceanic observations, RV "Sagar Kanya"; top inset: estuarine observations, fishing trawler; bottom inset: coastal observations, RV "Sagar Purvi".

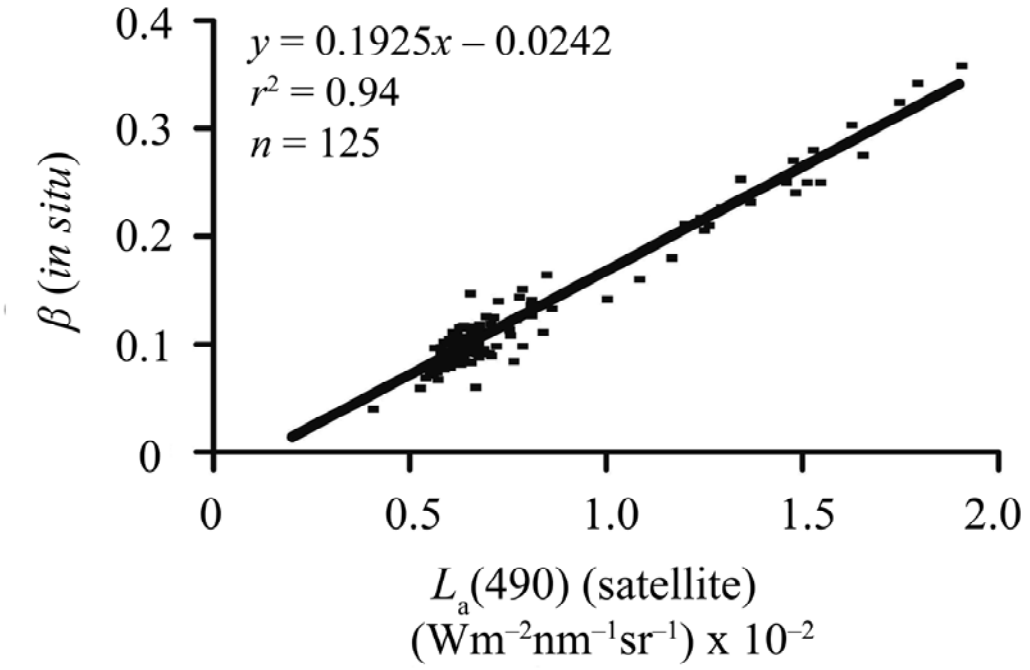

Figure 2. Regression between *in situ* β (Angstöm turbidity parameter) and satellite-derived L_a 490 (aerosol radiance at 490 nm).

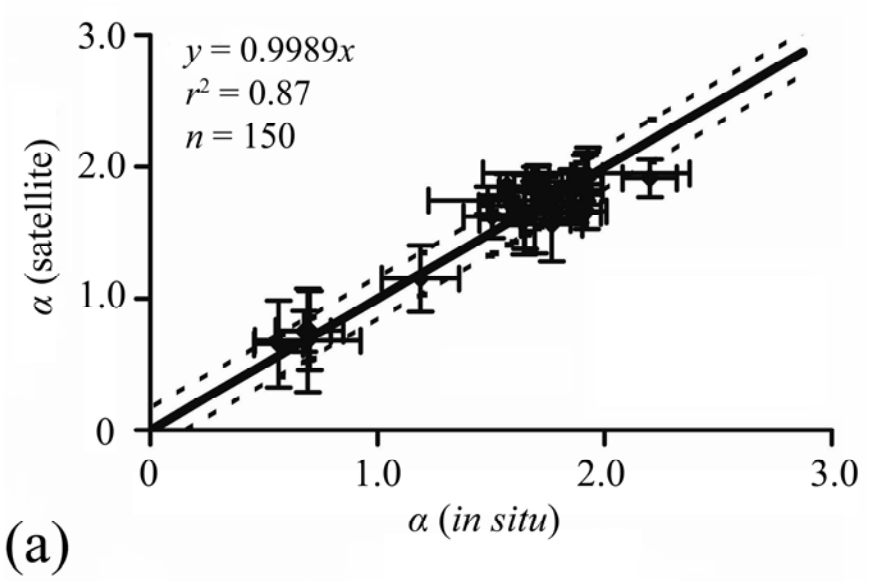
y = 0.9989x
r² = 0.87
n = 150
α (satellite)
α (in situ)
0
1.0
2.0
3.0

(a)

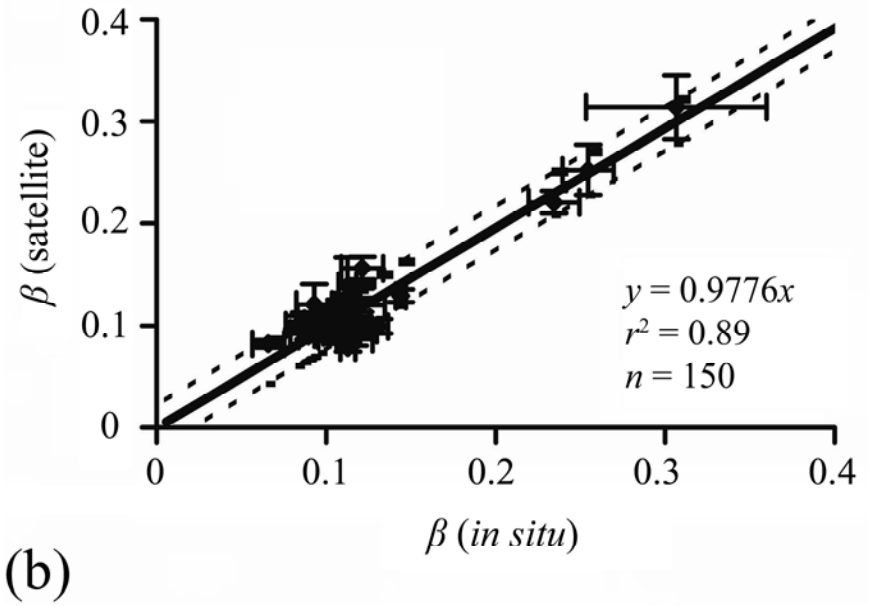
y = 0.9776x
r² = 0.89
n = 150
β (satellite)
β (in situ)
0
0.1
0.2
0.3
0.4

(b)

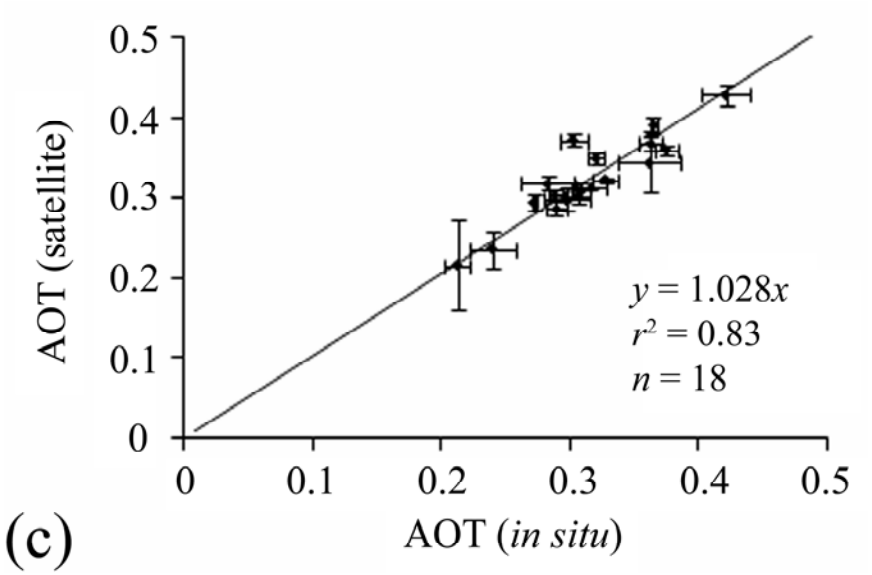

Figure 3. Correlation between (a) satellite- and *in situ*-derived α (aerosol size distribution parameter); (b) satellite-derived and *in situ* β (Angström turbidity parameter); (c) satellite-derived AOT and *in situ* values for validation. Dotted lines in (a) and (b) – 95% confidence level; vertical and horizontal bars – s.d.

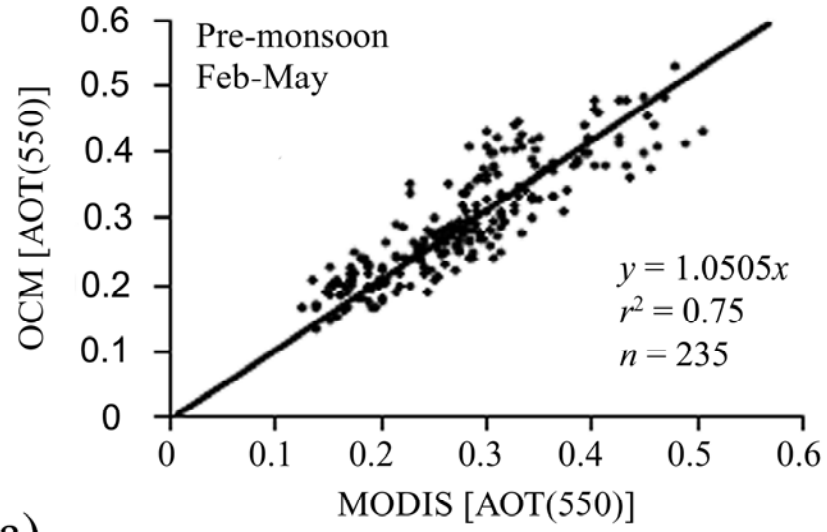
Pre-monsoon
Feb-May
$y = 1.0505x$
$r^2 = 0.75$
$n = 235$
OCM [AOT(550)]
MODIS [AOT(550)]
0
0.1
0.2
0.3
0.4
0.5
0.6

(a)

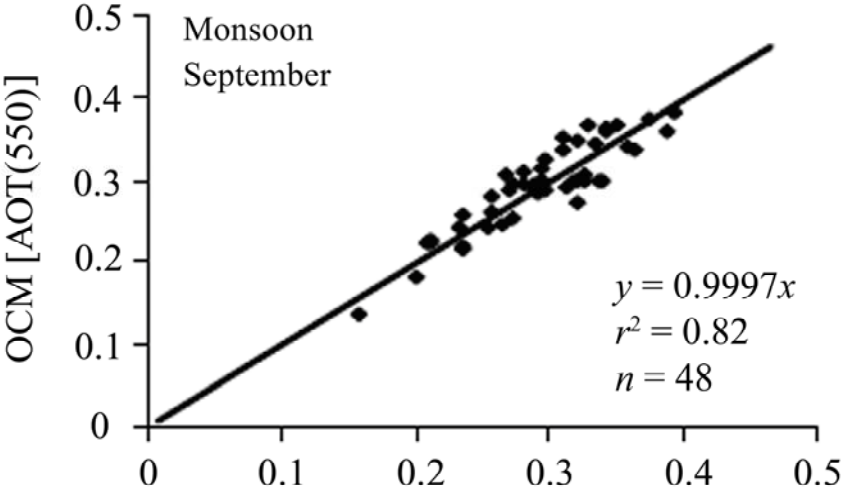
Monsoon
September
$y = 0.9997x$
$r^2 = 0.82$
$n = 48$
OCM [AOT(550)]
MODIS [AOT(550)]
0
0.1
0.2
0.3
0.4
0.5

(b)

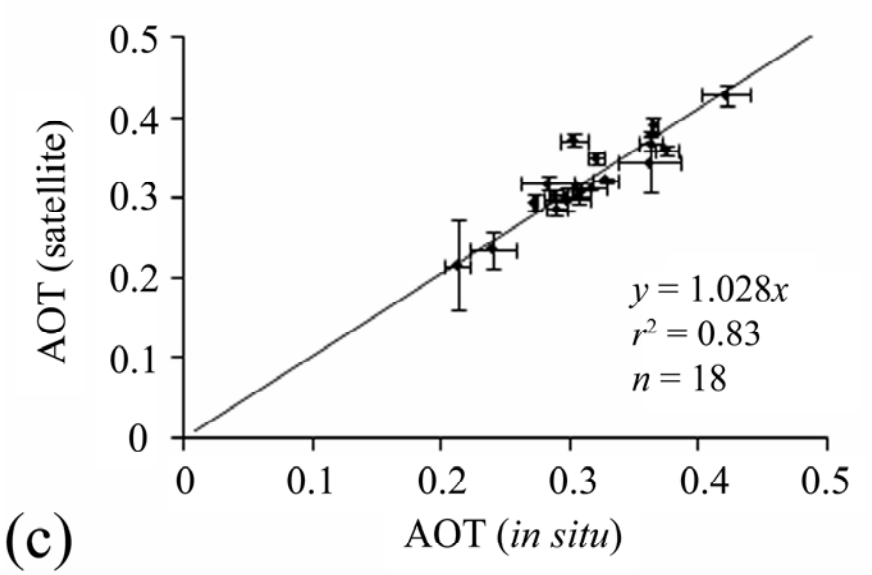

Figure 4. Correlation between AOT at 550 nm derived from OCM and MODIS for (a) pre-monsoon, (b) monsoon, and (c) post-monsoon seasons.

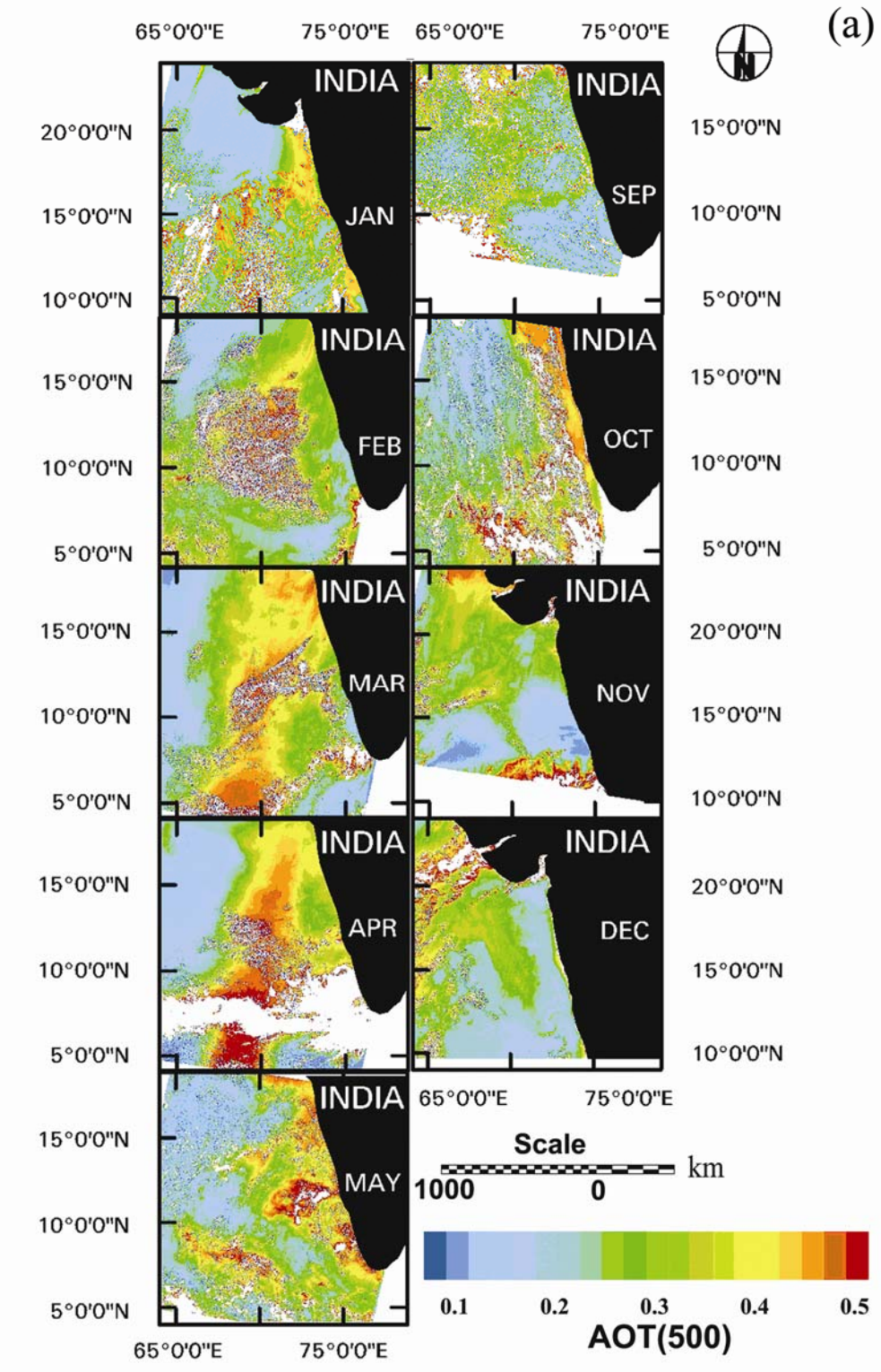
(a)
65°0'0"E
75°0'0"E
20°0'0"N
15°0'0"N
10°0'0"N
5°0'0"N
INDIA
JAN
FEB
MAR
APR
MAY
SEP
OCT
NOV
DEC
Scale
1000
0
km
0.1
0.2
0.3
0.4
0.5
AOT(500)

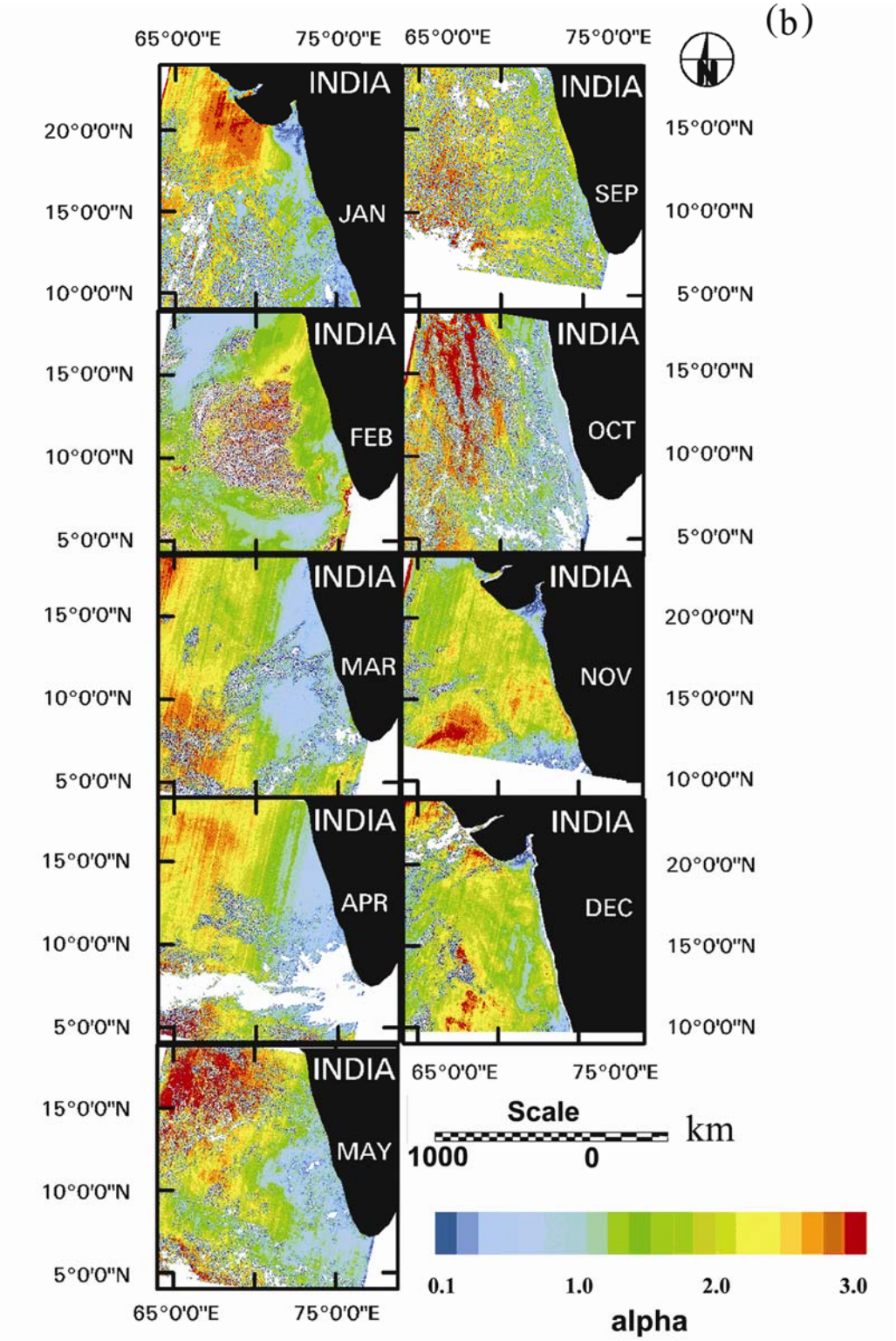

Figure 5. Spatial distribution of (a) AOT at 500 nm and (b) α derived with Ocean Colour Monitor (OCM) data for 10 January, 12 February, 18 March, 11 April, 11 May, 20 September, 6 October, 26 November, and 10 December 2005.